Engineering Science and Technology, an International Journal 22 (2019) 736–745

HOSTED BY

Contents lists available at ScienceDirect

Engineering Science and Technology, an International Journal

journal homepage: www.elsevier.com/locate/jestch

Full Length Article

# Histogram equalization techniques for enhancement of low radiance retinal images for early detection of diabetic retinopathy

Navdeep Singh [a,*], Lakhwinder Kaur [a], Kuldeep Singh [b]

[a] Dept. of Computer Sci. & Engg., Punjabi University, Patiala 147001, Punjab, India
[b] Central Research Lab, Bharat Electronics Ltd, Ghaziabad 201010, India

ARTICLE INFO

*Article history:*
Received 17 September 2018
Revised 7 January 2019
Accepted 28 January 2019
Available online 8 February 2019

*Keywords:*
Histogram equalization
Radiance
Retinal image enhancement
Entropy

ABSTRACT

Images are sometimes affected by improper illumination and are dark. This happens usually in medical images or the images acquired in low light conditions. This paper focuses on retinal imaging and proposes two techniques, RIHE-RVE (Radiance indicator based histogram equalization for retinal vessel enhancement) and RIHE-RRVE (Radiance indicator based histogram equalization for recursive retinal vessel enhancement) to address the problem of low light radiance. The techniques separate the histogram into sub-histograms at the split value determined by the tuneable parameter, $\psi$. RIHE-RVE recursively performs histogram integration after each split followed by equalization whereas in RIHE-RRVE histogram split can be done to any level (which is decided by the parameter,$r$) followed by equalization and integration. It has been observed from a comprehensive literature survey that very few algorithms exist that enhance the quality of retinal images. The proposed methods efficiently address the low light radiance problem. Performance evaluation of the techniques is done in terms of Information content (Entropy), PSNR (Peak signal to noise ratio), SSIM (Structure similarity index measurement), Euclidean distance and visual quality inspection. To demonstrate the robustness of the proposed methods, the techniques are not only applied specifically to publicly available retinal databases DRIVE, STARE and CHASE_DB1 but also to some of the MRI images taken from publicly available OASIS database. Results show that the proposed techniques outperform the state of the art techniques especially in low radiance images.


## 1. Introduction

Retinal diseases are on the rise in the working and aged population in all parts of the world. Diabetic retinopathy alone is the leading cause of blindness and it is estimated that people affected with diabetic retinopathy will rise from 126.6 million in 2011 to 191 million by 2030 [1,2]. Macular degeneration is another disease which is going to affect 196 million by 2020 which will further rise to 288 million by 2040 [3]. Not only the retinal diseases but other diseases such as diabetes mellitus [4], hypertension (a blood pressure elevation disease that is going to affect approximately 1.6 billion people around the world by the year 2025) [5] and stroke [6] can also be diagnosed by carefully examining the retinal image. The blood vascular structure plays a very important part in the diagnosis of diabetic retinopathy. Doctors can easily determine the stage of diabetic retinopathy just by inspecting the structure of the blood vessels, for example, the presence of tiny bulges and high tortuosity of the blood vessels indicate the beginning of diabetic retinopathy whereas the presence of many tiny blood vessels branching out of the main vessels indicates the presence of proliferative diabetic retinopathy [7], which is an advanced stage of diabetic retinopathy and is the cause of blindness in individuals.

In order to analyze the blood vessels, the vessels need to be extracted from the retina. Accurate segmentation of the blood vessels from the retina depend on the quality of the image. Unfortunately getting a high quality image is not always possible because of various factors such as the distance of the imaging device from the retina, movement of the eye ball and improper expansion of the eyelids etc. As a consequence, the retinal images suffer from low and non-uniform radiance. The main goal of this work is to address the issue of improper illumination in retinal images that happens during image acquisition. Overall, this paper focusses on the preprocessing step that deals with the improvement in the quality of the image in terms of illumination. This step of preprocessing plays a crucial role in the efficient and accurate segmentation of the blood vessels from the retina. A higher quality image leads to better vessel segmentation [8]. Various diseases such as diabetic retinopathy, hypertension etc. can be diagnosed

* Corresponding author.
*E-mail address:* navdeepsony@gmail.com (N. Singh).
Peer review under responsibility of Karabuk University.

https://doi.org/10.1016/j.jestch.2019.01.014
2215-0986/

by observing the changes in the structure of the retinal vessels [9]. Diabetic retinopathy if detected early can be treated in time and the patient can be saved from vision threatening irreversible problems. In this work, two techniques, RIHE-RVE (Radiance indicator based histogram equalization for retinal vessel enhancement) and RIHE-RRVE (Radiance indicator based histogram equalization for recursive retinal vessel enhancement) have been proposed to enhance the quality of images. In both the techniques, histogram is split based on the value of the tuneable parameter, $\psi$, that controls the level of enhancement. RIHE-RVE separates the histogram into two sub-histograms, equalizes both the histograms and then integrates them. This is done repeatedly depending on the difference between radiance values obtained from successive enhanced images. RIHE-RRVE recursively divides the histogram into multiple number of sub-histograms depending on the level decided by the parameter, $r$. In addition to the above techniques, a new technique for clipping the histogram has also been proposed. Histogram clipping is done in both the techniques based on the cumulative median value to avoid over enhancement. Just by changing the value of the tuneable parameter, $\psi$, level of enhancement can be controlled. The proposed techniques efficiently enhance the quality of low and non-uniformly illuminated images without any information loss. The techniques do not produce any unwanted artefacts, are robust in nature and can be applied to images of various types.

## 2. Related work

Accurate segmentation of the blood vessels is needed for diagnostic purposes and it can only be done if the image is clear and has high and uniform radiance. Very few techniques [10–13] have been developed that works on enhancing the quality of retinal images and out of them none focuses on low radiance retinal images as far as our knowledge is concerned. These techniques just focus on making the radiance uniform without taking into consideration the amount of radiance and the information content (entropy) already present in the image. It has been observed that even though the techniques succeed in getting a uniform radiance image but it comes at a cost of a high level loss of the entropy which is never desired especially in medical images as even a small loss of information content may lead to a totally different diagnosis. The proposed methods makes a conscious effort to take into account both the level of radiance and information content while enhancing the quality of retinal images to make them suitable for segmentation. Most of the techniques existing in literature that work on low radiance images focus on equalizing the histogram of the image in order to improve the visual quality of the image. Histogram equalization [14] is the most basic technique that equalizes an image by mapping the narrow range of intensity levels to the wider range of intensity levels available. This technique highly improves the radiance of the image but on the contrary it produces over enhancement in an image as a result of which crucial content information is lost. Over enhancement is produced because it always tends to change the mean brightness of the image to the middle of the intensity range available. The other limitation of histogram equalization is, it produces annoying artefacts rendering it in effective for most of the applications. BBHE (Brightness Preserving Bi-histogram Equalization) [15] addresses this limitation by dividing the original histogram into two sub-histograms on the basis of the mean of the image which are then equalized independently. The main advantage of this technique is that it preserves the mean of the enhanced image approximately equal to that of the original image besides suppressing annoying artefacts giving more realistic images. MMBEBHE (Minimum Mean Brightness Error Bi-histogram Equalization) [16] an extension of BBHE finds an optimal threshold value to separate the histogram into sub-histograms to perform image enhancement such that absolute mean brightness error is minimum. DSIHE (Dualistic Sub-image Histogram Equalization) [17] is another technique that performs the histogram division on the basis of median value rather than mean. High level of entropy is obtained using this technique. RMSHE (Recursive Mean Separate Histogram Equalization) [18] preserves mean brightness by recursively dividing the histogram into sub histograms producing a bright image. RSIHE (Recursive Sub-Image Histogram Equalization) [19] recursively divides the histogram into sub-histograms based on the sum of the cumulative probability density. RSWHE (Recursively Separated and Weighted Histogram Equalization) [20] modifies the sub histograms by weighting process based on power law function and then applies the process of histogram equalization on the sub histograms. BHEPL (Bi-histogram Equalization with a Plateau Limit for Digital Image Enhancement) [21] is another technique that divides the original histogram into two sub-histograms and clips the histograms based on the plateau value. This technique is very effective in terms of less computational time required to produce an enhanced image. DOTHE (Dominant Orientation-based Texture Histogram Equalization) [22] constructs the histogram based on the patches of the image that have dominant orientation. The main highlight of this technique is that as the pixels of the non- textured areas are not included, it helps in supressing the annoying artefacts that occur is histogram equalization techniques. RWMPHE (Recursive weighted multi-plateau histogram equalization) [23] subdivides the histogram into sub-histograms which are further clipped using various plateau limits. These sub-histograms are then equalized individually to get a higher quality image. QDHE (Quadrants Dynamic Histogram Equalization for Contrast Enhancement) [24] separates the histogram into four sub-histograms based on the median value of the input image. All the four quadrants are then clipped according to the input data mean and equalized. The technique gives good results without any noise amplification or over enhancement. Singh et al. [25] proposed techniques to improve the low exposure images. The techniques separate the histogram on the basis of the exposure value of the input image. SRHE (Sub-regions Histogram Equalization) [26] applies the Gaussian filter on the image to obtain smoothed intensity values which are then used to partition the image into histograms that are then equalized individually. Chaudhuri et al. [27] did the pioneer work that specifically focussed on retinal images. A $5 * 5$filter was used to reduce the effect of spurious noise present in the images but no attention was given to low and non-uniform radiance. Marin et al. [28] used $3 * 3$mean filter to reduce the noise followed by a Gaussian filter to further smooth the retinal image. Noise removal was followed by background homogenization to make the image radiance uniform. The technique to a certain extent was successful to get a uniform bright image but not without sacrificing a lot of information content of the image. Joshi et al. [29] proposed an enhancement technique for the improvement in the quality of non-uniformly illuminated dark images. They used the knowledge of imaging geometry and correction factor for removing the difference in the variability in the illumination of an image. Visual results obtained by this method were not very encouraging and presented a scope for improvement. Wan et al. [30] proposed adaptive histogram partition and brightness correction based infrared image enhancement method to enhance the quality of images. Grayscale density based metric was used to distinguish between foreground and background sub histograms. Foreground histograms were equalized using the local contrast based distribution to ensure a distinguishable difference between foreground and background pixels. In [31] a particle swarm optimization based local entropy based technique was proposed for histogram equal-

ization. The histogram was divided into sub histograms and particle swarm optimization was used to reduce over enhancement. Each sub histogram was equalized using the local entropy.

It has been observed that most of the equalization algorithms work on increasing the image contrast and very few focus on addressing the issue of improper illumination. Also majority of the existing techniques suffer from over enhancement as a result of which the information content is badly affected. In this work, the problem of improper illumination is addressed in such a way that overall information content is minimally affected. To ensure that the image is not over enhanced, a new histogram clipping algorithm is proposed based on which two techniques RIHE-RVE and RIHE-RRVE have been developed. The present paper is organized as follows: Section 3 describes the proposed algorithms, the results are presented in Section 4. The analysis of the proposed techniques is done in Section 5. Section 6 concludes the paper. The list of references is provided at the end of this article.

## 3. Proposed algorithms

The proposed algorithms determine the amount of under radiance that an image has and based on that performs the appropriate level of enhancement which results in a uniformly illuminated image with a very high value of entropy close to the original image. The techniques take care that under exposed regions are enhanced more than already high radiance regions. In the proposed work, a simple technique has been devised that can easily control the level of enhancement. For this purpose, a tuneable parameter $\psi$ is used to determine the split value that separates the histogram into sub histograms.

The split value, $B_v$ is calculated as depicted in Eqs. (1)–(4).

$$p_c(i) = h(i)/N \quad for\ \ 0 \le i \le L-1. \tag{1}$$

$$C(k) = \sum_{i=0}^{k} p_c(i) \quad for\ \ 0 \le k \le L-1. \tag{2}$$

$h$ is the histogram of the image, $N$ is the total number of pixels in the image,$L$ is the total number of intensity levels, $p_c$ and $C$ contains the normalized histogram counts and cummulative normalized histogram counts respectively of the input image. The value of the controlling parameter, $C_p$ is needed to be found such that

$$\sum_{j=0}^{C_p} C(j) \approx \psi \quad for\ any\ \ 0.1 \le \psi \le 0.9. \tag{3}$$

$$B_v = (L-1) - C_p - 1. \tag{4}$$

The value of tuneable parameter, $\psi$ decides the level of enhancement needed for an image. Lesser the value of $\psi$, more is the enhancement. This holds true because lesser value of $\psi$ will result in lower value of $C_p$as can be seen in Eq. (3). From Eq. (4), it can be induced that low $C_p$ will produce large split value, $B_v$ that separates the histogram into sub histograms. This process can be understood from the fact that for a low radiance image, pixel density of an image is more towards the lower intensity range of the histogram. Consequently, Eq. (3) can be satisfied with much lesser value of $C_p$ for a particular value of $\psi$ resulting in an extended first sub histogram. The first sub histogram is then equalized separately from the second sub histogram. Because of the extendedness of the sub histogram, a smaller intensity range of pixels of an input image is mapped to a much larger intensity range enhancing the low radiance region effectively. On the contrary, the second sub histogram has much lesser range and contains pixels that belong to the higher intensity range in an image. Because of the much smaller range, high end intensity pixels are therefore equalized in a much smaller range thus restricting over enhancement. In this work, three techniques have been proposed:

- Histogram Clipping
- RIHE-RVE
- RIHE-RRVE

### 3.1. Histogram clipping

Enhancing images often leads to the problem of over enhancement. In histogram clipping, a threshold value is used as the limiting value. The bin count greater than the threshold value is reduced to the threshold value to reduce the effect of over enhancement and get a more natural image. In this work, a new histogram clipping algorithm is proposed. Histogram is clipped based on the averaged median value which better reduces the effect of over enhancement.

#### 3.1.1. Pseudocode for histogram clipping

(1) Rearrange histogram values in the ascending order.
(2) Find unique values from the sorted list of values.
(3) Calculate median value, M from the set of unique values where median is the middle value if the number of unique values are odd or it is the mean value of the middle two values if the number of unique values are even.
(4) Calculate threshold value,

$$T_v = M/C_p \tag{5}$$

where $C_p$ is the controlling parameter found in Eq. (3). The value of $T_v$ must be rounded off to the nearest integer.

(5) The threshold value, $T_v$ found in Eq. (5) is used for clipping the histogram. All the values of the histogram, $h$ higher than $T_v$ are clipped to the value $T_v$ to create a new histogram, $h_N$. The values lower than the value of the threshold value, $T_v$ are not modified. This operation is shown in Eq. (6)

$$\text{Set}\ \ h_N = T_v \text{if} h(i) \ge T_v\ \ \text{else}\ \ h_N = h(i). \tag{6}$$

### 3.2. Radiance indicator based histogram equalization for retinal vessel enhancement (RIHE-RVE)

The algorithm calls itself recursively until the absolute difference between the successive radiance values, $\chi_1$ and $\chi_2$ (calculated using Eq. (7)) for input image and enhanced image respectively is less than the threshold error, $s$. In this work, value of $s$ is chosen to be 0.001. The threshold value,$s$, should be chosen carefully such that it should not be too high which might lead to high computational time and should not be too less to avoid under enhancement. Fig. 1 shows the flow chart of RIHE-RVE.

#### 3.2.1. Algorithm for RIHE-RVE

(1) Compute the histogram, $h$ for the input image, $f$, where a histogram contains the frequency of occurence of each intensity level.
(2) Compute the radiance value,

$$\chi_1 = \frac{\sum_{i=0}^{L-1} h(i).i}{L\sum_{i=0}^{L-1} h(i)}. \tag{7}$$

where $i$ represents the intensity value, $h(i)$ is the frequency of occurence of the intensity value $i$ and $L$ is the total number of inten-

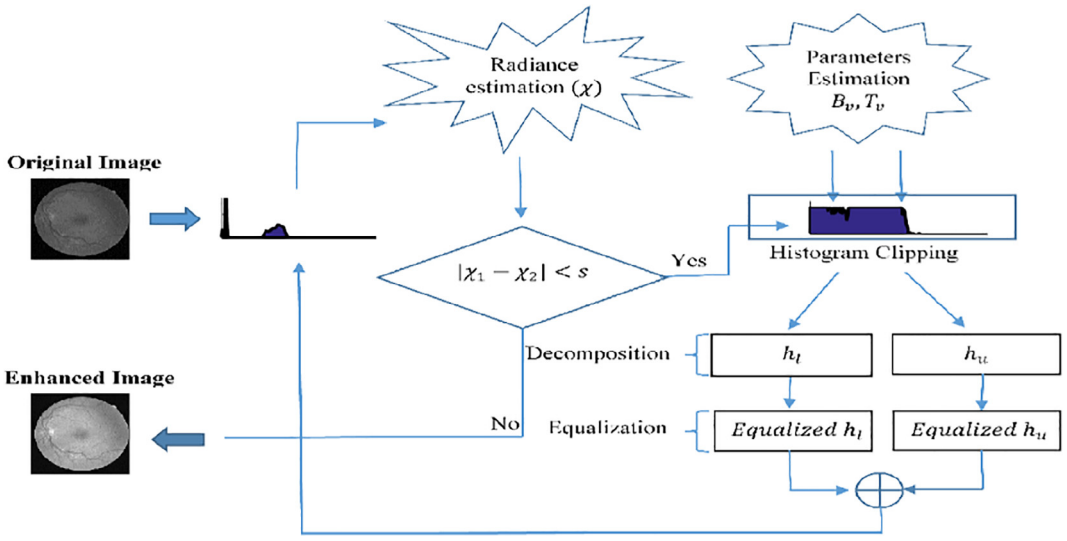


**Fig. 1.** Flowchart of RIHE-RVE technique.

sity levels, here $L = 256$. This equation determines the amount of exposure present in the image.

(3) Calculate the split value, $B_v$ from Eqs. (3) and (4) to divide the histogram in to sub histograms.
(4) Calculate the threshold value, $T_v$ from Eq. (5) for clipping the histogram to avoid over enhancement.
(5) Clip the histogram $h$ at threshold value $T_v$ to obtain clipped histogram$h_N$ from Eq. (6).
(6) Separate the clipped histogram $h_N$ into two sub-histograms $h_l$ and $h_u$ of intensity ranges 0 to $B_v$ and $B_{v+1}$ to $L-1$ respectively based on the split value $B_v$ calculated in step 3 of the algorithm.
(7) Equalize the two histograms $h_l$ and $h_u$ individually in their respective range of intensity. The darker regions will be enhanced more than the brighter regions.
(8) Integrate $h_l$ and $h_u$ to re-create the histogram, $h$.
(9) Repeat Step 2 to find the radiance value, $\chi_2$ of the equalized image.
(10) Apply steps 1–9 until the absolute difference between two consecutive radiance levels is less than the threshold error, $s$ as shown in $|\chi_1 - \chi_2| < s$.

### 3.3. Radiance indicator based histogram equalization for recursive retinal vessel enhancement (RIHE-RRVE)

RIHE-RRVE works by sub dividing the histogram into sub-histograms up to the chosen level of splitting,$r$. For$r = 1, 2^1 = 2$-sub-histograms will be obtained at level 1, for $r = 2, 2^2 = 4$histograms will be obtained at level 2 and for $r = n, 2^n$ sub-histograms will be obtained at level $n$ (maximum value of $n$ is chosen to be 7). The split values $B_{vl}$ and $B_{vu}$ for each of the sub-histograms are calculated as shown in Eqs. (8) and (9)

$$B_{vl} = B_v - (C_p * (1 - \chi_1)) - 1. \quad (8)$$

$$B_{vu} = h_{u_{max}} - (C_p * (1 - \chi_2)) - 1. \quad (9)$$

where $h_{u_{max}}$ denotes the maximum intensity value for the sub-histogram $h_u$. Fig. 2 shows the flow chart of RIHE-RRVE.

#### 3.3.1. Algorithm for RIHE-RRVE

(1) Compute the histogram, $h$ for the input image, $f$, where a histogram contains the frequency of occurence of each intensity level.
(2) Choose the level of splitting, $r$. Each histogram will be divided into two sub histograms iteratively upto the chosen level of decomposition. For the level, $r$, the number of sub histograms generated will be $2^r$. Each histogram will be divided as shown in steps 3–9 of this algorithm.
(3) Calculate the split value, $B_v$ using Eqs. (3) and (4) to divide the histogram in to sub histograms.
(4) Calculate the threshold value, $T_v$ using Eq. (5) for clipping the histogram to avoid over enhancement.
(5) Clip the histogram $h$ at threshold value $T_v$ to obtain clipped histogram$h_N$ from Eq. (6).
(6) Divide the clipped histogram into two sub-histograms $h_l$ and $h_u$ based on$B_v$ and compute newer split values $B_{vl}$ and $B_{vu}$ for $h_l$ and $h_u$ respectively from Eqs. (8) and (9). These split values are used to further divide the histograms $h_l$ and $h_u$ into sub histograms.
(7) Set $B_v = B_{vl}$to further sub divide $h_l$ in to $h_{l1}$ and $h_{l2}$. Once $h_l$ is divided into $h_{l1}$ and $h_{l2}$ sub histograms, compute $B_{vl}$ and $B_{vu}$ for $h_{l1}$ and $h_{l2}$ respectively from Eqs. (8) and (9) which will be further used to sub divide $h_{l1}$ and $h_{l2}$ into their respective sub histograms.
(8) Set $B_v = B_{vu}$to further sub divide $h_u$ in to $h_{u1}$ and $h_{u2}$. Once $h_u$ is divided into $h_{u1}$ and $h_{u2}$ sub histograms, compute $B_{vl}$ and $B_{vu}$ for $h_{u1}$ and $h_{u2}$ respectively from Eqs. (8) and (9) which will be further used to sub divide $h_{u1}$ and $h_{u2}$ into their respective sub histograms.
(9) Repeat the steps 7 and 8 to recursively separate the histograms in to sub-histograms up to the required level of splitting.
(10) Equalize all the sub-histogram individually in their respective range of intensities and integrate them to get the final equalized histogram.

The performance of both the techniques is affected by the change in the values of the parameters. RIHE-RVE depends on the tuneable parameter, $\psi$ whereas RIHE-RRVE depends on both

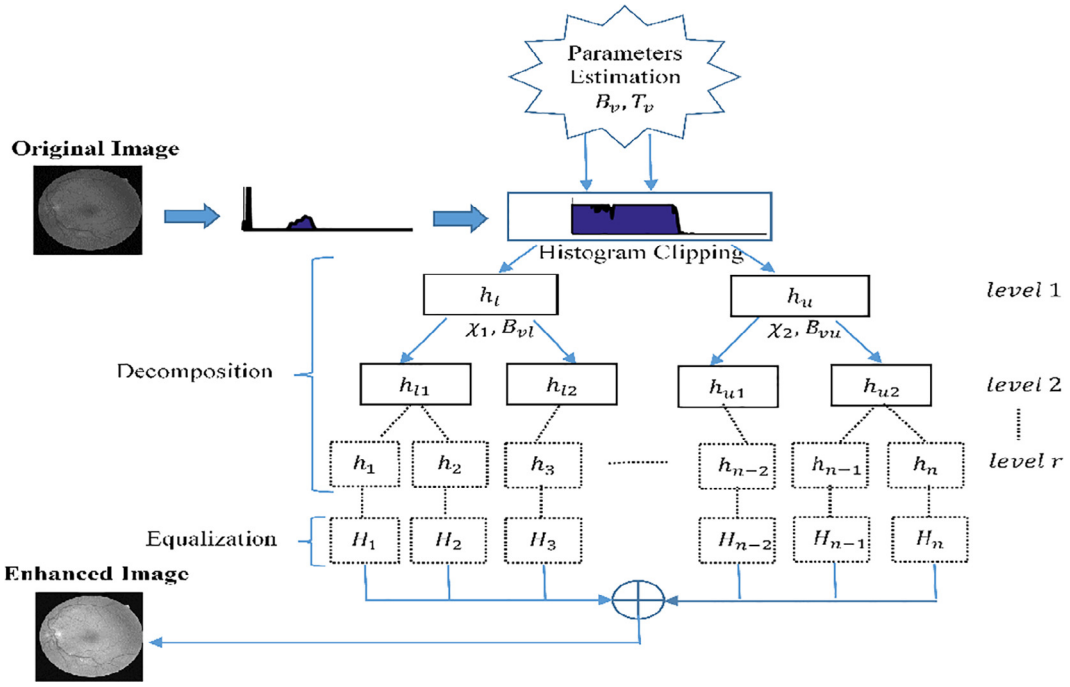


**Fig. 2.** Flowchart of RIHE-RRVE technique.

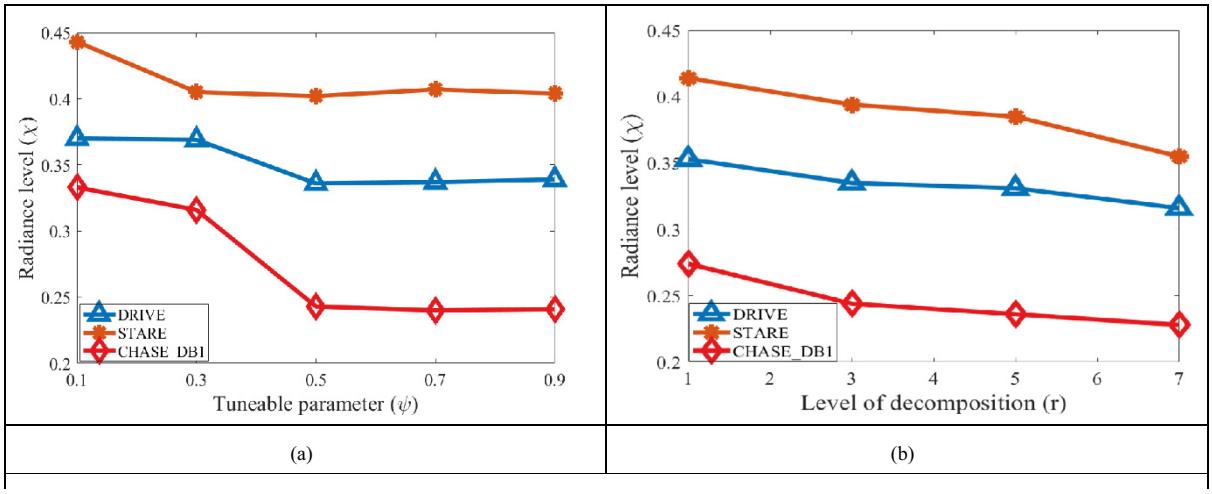


**Fig. 3.** (a) Effect of tuneable parameter '$\psi$' on the amount of radiance (RIHE-RVE) (b) Effect of split level '$r$' on the amount of radiance (RIHE-RRVE). The mean of radiance values obtained for different values of '$\psi$' for each level is used to calculate it.

the tuneable parameter, $\psi$ and level of splitting, $r$. The effect can be seen in Fig. 3.

## 4. Experimental results

In this section the results of the proposed methods are compared with the existing techniques i.e BBHE [15], BHEPL [21], DOTHE [22], RESIHE [25] and Marin et al. [28]. All the methods are robust in nature in the sense that they can be applied to any type of image except the last one which works specifically for retinal images.

### 4.1. Datasets used

To analyse the performance of the proposed methods, images from publicly available databases DRIVE [32], STARE [33], CHASE_DB1 [34] and OASIS [35,36] have been used. The DRIVE database contains 40 eye-fundus coloured images. These images are divided into two sets: training set and test set. Each of these sets contains 20 images each. The test set also contains the masks corresponding to each image in the test set. The STARE database contains 20 images, out of which 10 are pathological images. CHASE_DB1 database contains 28 retinal images of the children taken using the NM-200D fundus camera. Images were recorded in low light conditions using an illumination rating of 3. OASIS dataset contains both cross-sectional as well as longitudinal MRI images of young, middle aged, demented and non-demented older adults. The cross-sectional dataset contains images of 416 subjects whereas longitudinal dataset contains images of 150 subjects. While complete retinal databases have been used to find the overall results, only two images have been used from the OASIS database just to check the degree of robustness of the proposed techniques.

### 4.2. Performance evaluation based on visual inspection

The effectiveness of the methods can been seen in Figs. 4–7. Visual analysis shows that the images enhanced by the proposed methods have a high and uniform radiance such that the details are clearly visible. On the other hand, BBHE, RESIHE, BHEPL, DOTHE and MARIN ET AL. are able to increase the radiance of the images to a certain extent but the radiance is not uniform which can be easily seen in the seen images. There is a high level of radiance at the center of the images which gradually decreases towards the image boundary thus making the identification of pixel content impossible. Marine et al is able to provide uniform radiance but at the cost of high degree of information loss which is not acceptable in the medical domain.

### 4.3. Performance evaluation based on objective information

The algorithmic performance of the proposed methods has been measured in terms of Entropy, SSIM, PSNR and Euclidean distance. Entropy [20] measures the information content of the image.

Mathematical equation for entropy is:

$$E[p] = -\sum_{j=0}^{L-1} p(j) log_2 p(j). \tag{10}$$

where $E[p]$ is the entropy, $L$ is the number of intensity levels and $p$ contains the normalized histogram counts. Structure similarity index measurement (SSIM) [19,37] determines the change in the structural information of the image and is represented as following:

$$SSIM(x,y) = \frac{(2\mu_x\mu_y + c_1)(2\sigma_{xy} + c_2)}{(\mu_x^2 + \mu_y^2 + c_1)(\sigma_x^2 + \sigma_y^2 + c_2)}. \tag{11}$$

where $\mu_x$ and $\mu_y$ are the average of $x$ and $y$ respectively. $\sigma_x^2$ and $\sigma_y^2$ are variance of $x$ and $y$ respectively.$\sigma_{xy}$ is the covariance of $x$ and $y$. $c_1$ and $c_2$ are the two variables to stabilize the division with weak denominator where $c_1 = (k_1 L)^2$ and $c_2 = (k_2 L)^2$, $k_1 = 0.001$ and $k_2 = 0.003$. $L$ is the dynamic range of pixels.

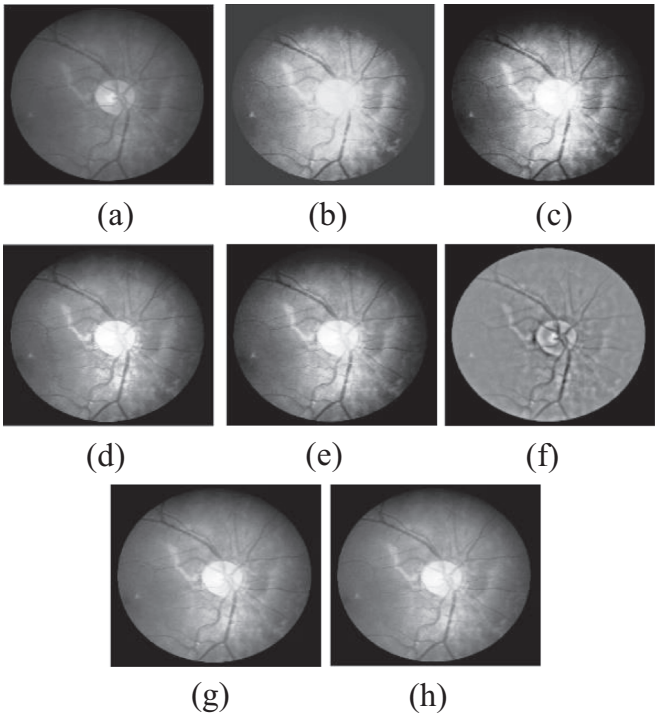


**Fig. 4.** (a) Original image (CHASE) (b) BBHE (c) DOTHE (d) RESIHE (e) BHEPL (f) Marin (g) RIHE-RVE ($\psi = 0.1$) (h) RIHE-RRVE($r = 1, \psi = 0.2$).

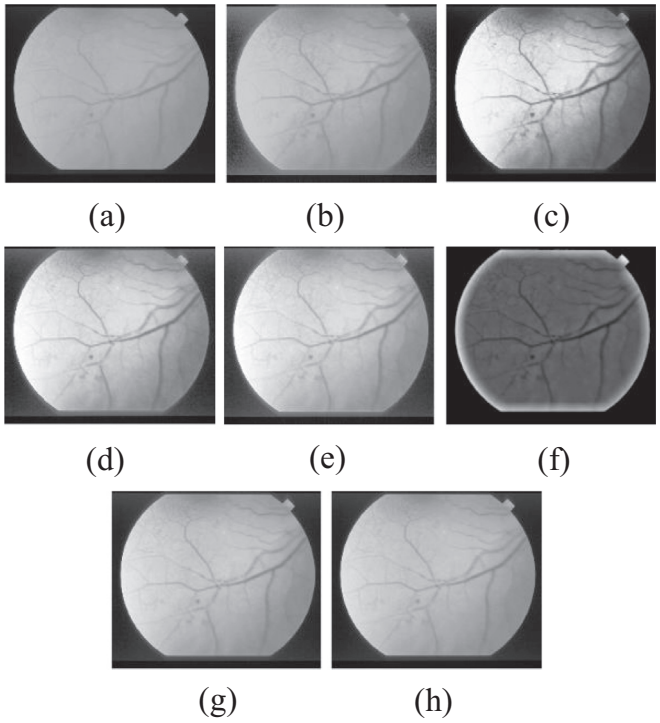


**Fig. 5.** (a) Original image (STARE) (b) BBHE (c) DOTHE (d) RESIHE (e) BHEPL (f) Marin (g) RIHE-RVE ($\psi = 0.1$) (h) RIHE-RRVE ($r = 1, \psi = 0.2$).

Peak signal to noise ratio (PSNR) [38] is the maximum intensity that a signal can have and it is denoted as:

$$PSNR = 10 log_{10} \frac{255^2}{\frac{1}{MN}\sum_{i,j}(g_{i,j} - f_{i,j})^2}. \tag{12}$$

where, $g$ is the enhanced image and $f$ is the original image. $M$ and $N$ denote the number of pixels row-wise and column-wise respectively.

Euclidean distance $d_E(x,y)$ [39] is given by

$$d_E^2(x,y) = \sum_{k=1}^{MN} (x^k - y^k)^2. \tag{13}$$

$x^k$ and $y^k$ are intensity values at corresponding locations $(k,l)$ of the two images $x$ and $y$.

It has been empirically found that RIHE-RVE gives a highly illuminated image with uniform radiance at $\psi = 0.1$ whereas for RIHE-RRVE, the optimal values are $r = 1$ and $\psi = 0.2$. Fig. 2 shows the effect of '$\psi$' and '$r$' on the level of radiance for different retinal databases.It can be observed from Figs. 4–7 that there is no over enhancement in images enhanced by the proposed techniques in contrary to some of the existing techniques. Results of various methods using two random images from each database are tabulated in Tables 1–4 (where 1st pair of images belongs to the CHASE dataset, 2nd pair belongs to DRIVE, 3rd to STARE and 4th to OASIS dataset).

Average results in terms of Entropy, SSIM, PSNR and Euclidean distance are presented in Tables 5–7. The average results are obtained only for retinal images using all the test images of various retinal datasets. A high value of entropy as close as possible to the original image is desired. Higher value of SSIM and lower value of Euclidean distance indicates that the image is closer to the original

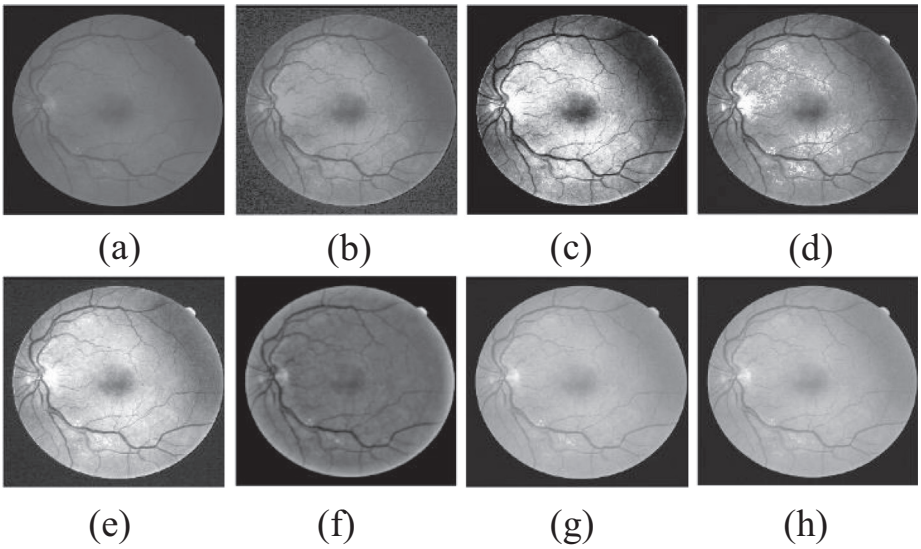


**Fig. 6.** (a) Original image (DRIVE) (b) BBHE (c) DOTHE (d) RESIHE (e) BHEPL (f) Marin (g) RIHE-RVE ($\psi = 0.1$) (h) RIHE-RRVE ($r = 1, \psi = 0.2$).

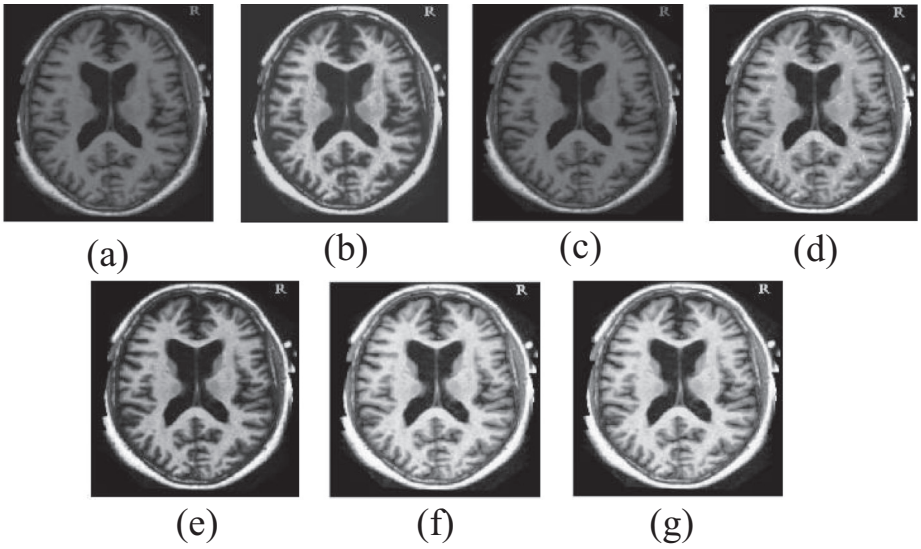


**Fig. 7.** MRI images have been taken to test the robustness of the proposed techniques. (a) Original image (OASIS) (b) BBHE (c) DOTHE (d) RESIHE (e) BHEPL (f) RIHE-RVE ($\psi = 0.1$) (g) RIHE-RRVE ($r = 1, \psi = 0.2$) (Marin et al. work only for retinal images).

**Table 1**
Performance comparison based on Entropy.

| Images | Original | BBHE | RESIHE | BHEPL | DOTHE | MARIN | RIHE-RVE | RIHE-RRVE |
|---|---|---|---|---|---|---|---|---|
| Image 1 | 5.752 | 5.467 | 5.654 | 5.661 | 5.448 | 4.006 | **5.719** | **5.719** |
| Image 2 | 5.782 | 5.575 | 5.678 | 5.702 | 5.564 | 4.168 | **5.758** | **5.758** |
| Image 3 | 5.302 | 5.199 | 5.264 | 5.277 | 4.976 | 3.991 | **5.302** | **5.302** |
| Image 4 | 5.510 | 5.379 | 5.453 | 5.468 | 5.160 | 4.259 | **5.509** | **5.509** |
| Image 5 | 6.549 | 6.453 | 6.493 | 6.503 | 6.268 | 3.993 | **6.544** | **6.546** |
| Image 6 | 6.530 | 6.446 | 6.490 | 6.495 | 6.239 | 4.247 | **6.523** | **6.526** |
| Image 7 | 6.182 | 5.809 | 6.077 | **6.093** | 5.921 | – | 6.060 | 6.060 |
| Image 8 | 6.416 | 6.124 | 6.345 | 6.343 | 6.257 | – | **6.380** | **6.408** |

image. A higher value of PSNR indicates the presence of lesser noise. The running time comparison of various algorithms has been made in Table 8. The time has been calculated by executing each algorithm 10 times and taking the average of the time taken to execute the algorithm. RIHE_RRVE records the lowest running time of 17 ms whereas RIHE_RVE records high running time of 38 ms. Large running time of RIHE_RVE is due to the iterative nature of the algorithm as the algorithm goes on equalizing the image until the difference between consecutive radiance levels becomes greater than the threshold error.

**Table 2**
Performance comparison based on SSIM.

| Images | BBHE | RESIHE | BHEPL | DOTHE | MARIN | RIHE-RVE | RIHE-RRVE |
|---|---|---|---|---|---|---|---|
| Image 1 | 0.492 | 0.787 | **0.826** | 0.742 | 0.784 | 0.786 | 0.787 |
| Image 2 | 0.536 | 0.821 | 0.840 | 0.792 | 0.820 | **0.847** | **0.848** |
| Image 3 | 0.381 | 0.657 | 0.516 | 0.443 | 0.635 | **0.790** | **0.801** |
| Image 4 | 0.392 | 0.738 | 0.546 | 0.461 | 0.638 | **0.933** | **0.934** |
| Image 5 | 0.755 | 0.836 | 0.825 | 0.759 | 0.596 | **0.967** | **0.983** |
| Image 6 | 0.756 | 0.836 | 0.836 | 0.754 | 0.575 | **0.939** | **0.963** |
| Image 7 | 0.514 | 0.723 | **0.795** | 0.567 | – | 0.606 | 0.608 |
| Image 8 | 0.530 | 0.625 | 0.789 | 0.525 | – | 0.591 | **0.793** |

**Table 3**
Performance comparison based on PSNR.

| Images | BBHE | RESIHE | BHEPL | DOTHE | MARIN | RIHE-RVE | RIHE-RRVE |
|---|---|---|---|---|---|---|---|
| Image 1 | 12.292 | **16.839** | 16.642 | 14.494 | 13.715 | 16.444 | 16.537 |
| Image 2 | 13.077 | **21.784** | 17.521 | 15.300 | 14.771 | 21.477 | 21.616 |
| Image 3 | 10.725 | 16.370 | 11.407 | 12.581 | **23.275** | 12.724 | 12.840 |
| Image 4 | 11.021 | 19.619 | 12.705 | 12.972 | **20.308** | 19.510 | 19.651 |
| Image 5 | 15.062 | 17.300 | 15.439 | 16.298 | 12.754 | **26.953** | **29.875** |
| Image 6 | 15.254 | 18.443 | 17.238 | 16.219 | 12.032 | **23.138** | **25.088** |
| Image 7 | 13.284 | 14.745 | **16.298** | 12.092 | – | 11.214 | 11.277 |
| Image 8 | 12.002 | 13.381 | 16.964 | 10.495 | – | 12.763 | **18.073** |

**Table 4**
Performance comparison based on Euclidean distance.

| Images | BBHE | RESIHE | BHEPL | DOTHE | MARIN | RIHE-RVE | RIHE-RRVE |
|---|---|---|---|---|---|---|---|
| Image 1 | 0.413 | 0.411 | 0.406 | **0.080** | 0.191 | 0.411 | 0.411 |
| Image 2 | 0.411 | 0.407 | 0.403 | **0.079** | 0.166 | 0.406 | 0.406 |
| Image 3 | 0.285 | **0.281** | 0.287 | 0.328 | 0.394 | 0.292 | 0.292 |
| Image 4 | 0.271 | **0.262** | 0.272 | 0.309 | 0.374 | 0.263 | 0.263 |
| Image 5 | 0.126 | 0.132 | 0.129 | 0.143 | 0.363 | **0.095** | **0.085** |
| Image 6 | 0.130 | 0.125 | 0.126 | 0.143 | 0.351 | **0.109** | **0.094** |
| Image 7 | 0.313 | 0.309 | **0.307** | 0.321 | – | 0.311 | 0.311 |
| Image 8 | **0.154** | 0.174 | 0.156 | 0.168 | – | 0.177 | 0.166 |

**Table 5**
Average results for DRIVE database.

| Statistical Index | BBHE | RESIHE | BHEPL | DOTHE | MARIN | RIHE-RVE | RIHE-RRVE |
|---|---|---|---|---|---|---|---|
| Entropy | 5.572 | 5.648 | 5.672 | 5.348 | 4.316 | **5.717** | **5.727** |
| SSIM | 0.478 | 0.775 | 0.638 | 0.508 | 0.627 | **0.964** | **0.968** |
| PSNR | 12.806 | 20.263 | 15.140 | 14.567 | 19.491 | **29.336** | **30.474** |
| Euclidean | 0.256 | 0.236 | 0.255 | 0.294 | 0.372 | **0.198** | **0.194** |

**Table 6**
Average results for STARE database.

| Statistical Index | BBHE | RESIHE | BHEPL | DOTHE | MARIN | RIHE-RVE | RIHE-RRVE |
|---|---|---|---|---|---|---|---|
| Entropy | 6.628 | 6.672 | 6.702 | 6.365 | 4.370 | **6.733** | **6.761** |
| SSIM | 0.766 | 0.893 | 0.856 | 0.659 | 0.633 | **0.967** | **0.976** |
| PSNR | 15.014 | 22.304 | 16.791 | 15.640 | 16.256 | **26.435** | **27.789** |
| Euclidean | 0.119 | 0.097 | 0.113 | 0.147 | 0.322 | **0.082** | **0.071** |

**Table 7**
Average results for CHASE database.

| Statistical Index | BBHE | RESIHE | BHEPL | DOTHE | MARIN | RIHE-RVE | RIHE-RRVE |
|---|---|---|---|---|---|---|---|
| Entropy | 5.479 | 5.610 | 5.634 | 5.459 | 4.061 | **5.665** | **5.665** |
| SSIM | 0.516 | 0.808 | 0.811 | 0.761 | 0.805 | 0.806 | **0.814** |
| PSNR | 12.548 | **20.615** | 16.616 | 15.256 | 16.271 | 17.671 | 17.783 |
| Euclidean | **0.415** | 0.411 | 0.410 | 0.086 | 0.173 | 0.412 | 0.412 |

**Table 8**
Comparison of average running time of various methods.

| Method | Running time (ms) |
|---|---|
| BBHE | 30 |
| RESIHE | 18 |
| BHEPL | 29 |
| DOTHE | 53 |
| MARIN | 29 |
| RIHE-RVE | 38 |
| RIHE-RRVE | **17** |

## 5. Discussion

The proposed techniques work using divide and conquer algorithm, separating the histogram into sub histograms which are then equalized locally to avoid over enhancement. The techniques can effectively enhance the quality of an image and this high quality image is used in computer aided diagnosis (CAD) of diabetic retinopathy. In CAD, the vessels are automatically extracted from the enhanced image. The blood vascular structure is then studied to ascertain the severity of the disease. If the vascular structure has bulges in it and has high tortuosity, it gives an early indication of the beginning of diabetic retinopathy which if not treated timely can lead to severe diabetic retinopathy which may even cause permanent blindness. The proposed work focusses on the enhancement of retinal images and there are certain important aspects associated with it. Among them, the most important is choosing the correct split value to separate the histogram into sub histograms for illuminating the under exposed regions. The most significant aspect associated with the techniques is that not all the portions of the image are equally enhanced rather the darker regions are illuminated more in comparison to the already illuminated regions. Experimental results demonstrate that a higher level of radiance can be achieved for lower values of the parameter $\psi$ but the amount of illumination attained in the image comes at the cost of information. A higher level of illumination results in higher information loss and this loss in information can be reduced by fine tuning the parameter, $\psi$. It has been observed that a higher value of the tuneable parameter results in minimum information loss. Further, it has been observed that the proposed techniques not only provide better uniform illumination but also retains maximum information than the existing state of the art methods even at the lowest value of the tuneable parameter. The threshold error, $s$ also plays a very important role in controlling the amount of radiance in the image. A higher value of $s$ results in over enhancement of the image and a lower values results in under enhancement. Therefore, an optimal value needs to be chosen to perform the right amount of enhancement in the image. A sincere effort has been made to ascertain the effect of the level of decomposition on the amount of illumination and it has been observed that as the level of decomposition increases the amount of illumination decreases. Furthermore, the information loss also decreases with the increase in the level of decomposition of the histogram. It has been observed that the techniques are affected by the variation in the amount of intensity levels in the background of the image. This effect can be seen on the CHASE_DB1 dataset (it contains images of persons belonging to different ethnicity with highly varied background images) as shown in the Table 7. Still the proposed techniques are able to perform better in terms of two metrics, Entropy and SSIM. No existing technique exhibit superior performance on this dataset in terms of the majority of metrics. We are highly motivated to address this issue in the future work. The results support the fact that the techniques are robust in nature and are efficient in handling different types of images.

## 6. Conclusion

Diabetic retinopathy can be diagnosed by examining the retinal vascular structure of the fundus image of a patient. In order to inspect the vascular structure, first of all it needs to be extracted from the retina through an automatic process as manual segmentation is a very time consuming process. Accurate segmentation or extraction of the retinal vascular structure can only be done if the image is of high quality. Generally, retinal images are affected with improper illumination which occurs during image acquisition and it leads to improper extraction of the blood vessels from the retina. Inappropriate extraction sometimes leads to wrong diagnosis of the disease which can be life threatening. In this paper, two tuneable enhancement techniques, RIHE-RVE and RIHE-RRVE have been proposed to address the problem of non uniform illumination in retinal images to make the images better suited for computer aided diagnosis (CAD). To avoid over enhancement a new histogram clipping algorithm has also been proposed. Performance metrics show that the proposed techniques outperforms most of the state of the art techniques. The future work will focus on the extension of the proposed techniques for 3D retinal and MRI scans.

## References

[1] N. Congdon, Y. Zheng, M. He, The worldwide epidemic of diabetic retinopathy, Indian J. Ophthalmol. 60 (2012) 428, https://doi.org/10.4103/0301-4738.100542.
[2] J.W.Y. Yau, S.L. Rogers, R. Kawasaki, E.L. Lamoureux, J.W. Kowalski, T. Bek, S.-J. Chen, J.M. Dekker, A. Fletcher, J. Grauslund, S. Haffner, R.F. Hamman, M.K. Ikram, T. Kayama, B.E.K. Klein, R. Klein, S. Krishnaiah, K. Mayurasakorn, J.P. O'Hare, T.J. Orchard, M. Porta, M. Rema, M.S. Roy, T. Sharma, J. Shaw, H. Taylor, J.M. Tielsch, R. Varma, J.J. Wang, N. Wang, S. West, L. Xu, M. Yasuda, X. Zhang, P. Mitchell, T.Y. Wong, Global prevalence and major risk factors of diabetic retinopathy, Diab. Care 35 (2012) 556–564, https://doi.org/10.2337/dc11-1909.
[3] W.L. Wong, X. Su, X. Li, C.M.G. Cheung, R. Klein, C.-Y. Cheng, T.Y. Wong, Global prevalence of age-related macular degeneration and disease burden projection for 2020 and 2040: a systematic review and meta-analysis, Lancet Glob. Heal. 2 (2014) e106–e116, https://doi.org/10.1016/S2214-109X(13)70145-1.
[4] M.D. Ning Cheung, M.D. Prof Paul Mitchell, M.D. Tien Yin Wong, Diabetic retinopathy, Lancet J. 376 (2010) 124–136.
[5] R. Chen, K. Dharmarajan, V.T. Kulkarni, N. Punnanithinont, A. Gupta, B. Bikdeli, P.S. Mody, I. Ranasinghe, Most important outcomes research papers on hypertension, Circ. Cardiovasc. Qual. Outcomes 6 (2013), https://doi.org/10.1161/CIRCOUTCOMES.113.000424.
[6] L. Konstantinidis, Y. Guex-Crosier, Hypertension and the eye, Curr. Opin. Ophthalmol. (2016), https://doi.org/10.1097/ICU.0000000000000307.
[7] M.M. Nentwich, Diabetic retinopathy – ocular complications of diabetes mellitus, World J. Diab. 6 (2015) 489, https://doi.org/10.4239/wjd.v6.i3.489.
[8] M. Javidi, H.-R. Pourreza, A. Harati, Vessel segmentation and microaneurysm detection using discriminative dictionary learning and sparse representation, Comput. Meth. Prog. Biomed. 139 (2017) 93–108, https://doi.org/10.1016/j.cmpb.2016.10.015.
[9] H. Safi, S. Safi, A. Hafezi-Moghadam, H. Ahmadieh, Early detection of diabetic retinopathy, Surv. Ophthalmol. 63 (2018) 601–608, https://doi.org/10.1016/j.survophthal.2018.04.003.
[10] P. Feng, Y. Pan, B. Wei, W. Jin, D. Mi, Enhancing retinal image by the Contourlet transform, Pattern Recognit. Lett. 28 (2007) 516–522, https://doi.org/10.1016/j.patrec.2006.09.007.
[11] S.H. Rezatofighi, A. Roodaki, H. Ahmadi Noubari, An enhanced segmentation of blood vessels in retinal images using contourlet, in: 2008 30th Annu. Int. Conf. IEEE Eng. Med. Biol. Soc., IEEE, 2008, pp. 3530–3533, https://doi.org/10.1109/IEMBS.2008.4649967.
[12] P.S. Chandra, M.C. Hanumantharaju, M.T. Gopalakrishna, Retinal based image enhancement using contourlet transform, in: Proc. 3rd Int. Conf. Front. Intell. Comput. Theory Appl., 2015, pp. 581–587.
[13] M.U. Akram, A. Atzaz, S.F. Aneeque, S.A. Khan, Blood vessel enhancement and segmentation using wavelet transform, in: 2009 Int. Conf. Digit. Image Process, IEEE, 2009, pp. 34–38, https://doi.org/10.1109/ICDIP.2009.70.
[14] R.C. Gonzalez, R.E. Woods, B.R. Masters, Digital Image Processing, Third Edition, J. Biomed. Opt. 14 (2009), https://doi.org/10.1117/1.3115362.
[15] Yeong-Taeg Kim, Contrast enhancement using brightness preserving bi-histogram equalization, IEEE Trans. Consum. Electron. 43 (1997) 1–8, https://doi.org/10.1109/30.580378.
[16] Soong-Der Chen, A.R. Ramli, Minimum mean brightness error bi-histogram equalization in contrast enhancement, IEEE Trans. Consum. Electron. 49 (2003) 1310–1319, https://doi.org/10.1109/TCE.2003.1261234.
[17] Yu Wang, Qian Chen, Baeomin Zhang, Image enhancement based on equal area dualistic sub-image histogram equalization method, IEEE Trans. Consum. Electron. 45 (1999) 68–75, https://doi.org/10.1109/30.754419.

[18] Soong-Der Chen, A.R. Ramli, Contrast enhancement using recursive mean-separate histogram equalization for scalable brightness preservation, IEEE Trans. Consum. Electron. 49 (2003) 1301–1309, https://doi.org/10.1109/TCE.2003.1261233.
[19] K.S. Sim, C.P. Tso, Y.Y. Tan, Recursive sub-image histogram equalization applied to gray scale images, Pattern Recognit. Lett. 28 (2007) 1209–1221, https://doi.org/10.1016/j.patrec.2007.02.003.
[20] M. Kim, M.G. Chung, Recursively separated and weighted histogram equalization for brightness preservation and contrast enhancement, IEEE Trans. Consum. Electron. 54 (2008) 1389–1397, https://doi.org/10.1007/s10055-013-0226-9.
[21] C. Ooi, N. Pik Kong, H. Ibrahim, Bi-histogram equalization with a plateau limit for digital image enhancement, IEEE Trans. Consum. Electron. 55 (2009) 2072–2080, https://doi.org/10.1109/TCE.2009.5373771.
[22] K. Singh, D.K. Vishwakarma, G.S. Walia, R. Kapoor, Contrast enhancement via texture region based histogram equalization, J. Mod. Opt. 63 (2016) 1444–1450, https://doi.org/10.1080/09500340.2016.1154194.
[23] M.A. Qadar, Y. Zhaowen, A. Rehman, M.A. Alvi, Recursive weighted multi-plateau histogram equalization for image enhancement, Optik (Stuttg). 126 (2015) 5890–5898, https://doi.org/10.1016/j.ijleo.2015.08.278.
[24] C. Ooi, N. Mat Isa, Quadrants dynamic histogram equalization for contrast enhancement, IEEE Trans. Consum. Electron. 56 (2010) 2552–2559, https://doi.org/10.1109/TCE.2010.5681140.
[25] K. Singh, R. Kapoor, S.K. Sinha, Enhancement of low exposure images via recursive histogram equalization algorithms, Optik (Stuttg). 126 (2015) 2619–2625, https://doi.org/10.1016/j.ijleo.2015.06.060.
[26] H. Ibrahim, N. Pik Kong, Image sharpening using sub-regions histogram equalization, IEEE Trans. Consum. Electron. 55 (2009) 891–895, https://doi.org/10.1109/TCE.2009.5174471.
[27] S. Chaudhuri, S. Chatterjee, N. Katz, M. Nelson, M. Goldbaum, Detection of blood vessels in retinal images using two-dimensional matched filters, IEEE Trans. Med. Imag. 8 (1989) 263–269, https://doi.org/10.1109/42.34715.
[28] D. Marín, A. Aquino, M.E. Gegundez-Arias, J.M. Bravo, A new supervised method for blood vessel segmentation in retinal images by using gray-level and moment invariants-based features, IEEE Trans. Med. Imag. 30 (2011) 146–158, https://doi.org/10.1109/TMI.2010.2064333.
[29] G.D. Joshi, J. Sivaswamy, Colour retinal image enhancement based on domain knowledge, in: 2008 Sixth Indian Conf. Comput. Vision, Graph. Image Process, IEEE, 2008, pp. 591–598, https://doi.org/10.1109/ICVGIP.2008.70.
[30] M. Wan, G. Gu, W. Qian, K. Ren, Q. Chen, X. Maldague, Infrared image enhancement using adaptive histogram partition and brightness correction, Rem. Sens. 10 (2018) 682, https://doi.org/10.3390/rs10050682.
[31] M. Wan, G. Gu, W. Qian, K. Ren, Q. Chen, X. Maldague, Particle swarm optimization-based local entropy weighted histogram equalization for infrared image enhancement, Infrared Phys. Technol. 91 (2018) 164–181, https://doi.org/10.1016/j.infrared.2018.04.003.
[32] J. Staal, M.D. Abràmoff, M. Niemeijer, M.A. Viergever, B. Van Ginneken, Ridge-based vessel segmentation in color images of the retina, IEEE Trans. Med. Imag. (2004), https://doi.org/10.1109/TMI.2004.825627.
[33] A. Hoover, M. Hoover, A. Kouznetsova, V. Goldbaum, A. Hoover, Locating blood vessels in retinal images by piecewise threshold probing of a matched filter response, IEEE Trans. Med. Imag. 19 (2000) 203–210, https://doi.org/10.1109/42.845178.
[34] M.M. Fraz, P. Remagnino, A. Hoppe, B. Uyyanonvara, A.R. Rudnicka, C.G. Owen, S.A. Barman, An ensemble classification-based approach applied to retinal blood vessel segmentation, IEEE Trans. Biomed. Eng. 59 (2012) 2538–2548, https://doi.org/10.1109/TBME.2012.2205687.
[35] D.S. Marcus, A.F. Fotenos, J.G. Csernansky, J.C. Morris, R.L. Buckner, Open access series of imaging studies: longitudinal MRI data in nondemented and demented older adults, J. Cogn. Neurosci. 22 (2010) 2677–2684, https://doi.org/10.1162/jocn.2009.21407.
[36] D.S. Marcus, T.H. Wang, J. Parker, J.G. Csernansky, J.C. Morris, R.L. Buckner, Open access series of imaging studies (OASIS): cross-sectional MRI data in young, middle aged, nondemented, and demented older adults, J. Cogn. Neurosci. 19 (2007) 1498–1507, https://doi.org/10.1162/jocn.2007.19.9.1498.
[37] S.A. El said, Enhanced ultrasound images denoising technique, Int. J. Biomed. Eng. Technol. 10 (2012) 185, https://doi.org/10.1504/IJBET.2012.049368.
[38] R.H. Chan, Chung-Wa, M. Nikolova, Salt-and-pepper noise removal by median-type noise detectors and detail-preserving regularization, IEEE Trans. Image Process. 14 (2005) 1479–1485, https://doi.org/10.1109/TIP.2005.852196.
[39] L. Wang, Y. Zhang, J. Feng, On the Euclidean distance of images, IEEE Trans. Pattern Anal. Mach. Intell. (2005), https://doi.org/10.1109/TPAMI.2005.165.